Nanoscale Advances

PAPER

View Article Online
View Journal | View Issue

Cite this: *Nanoscale Adv.*, 2019, **1**, 3699

Plasmonic coloration of silver nanodome arrays for a smartphone-based plasmonic biosensor†

Mana Toma ‡* and Keiko Tawa

In this study, the utility of plasmonic coloration on silver nanodome arrays for sensitive and quantitative detection of biomolecules using a smartphone-based sensor is proposed. In particular, a quantitative analysis of DNA hybridization was achieved using the hue angle in the HSV color space obtained from a photograph of a sensing spot taken using a smartphone camera. Silver and gold nanodome arrays consisting of a polystyrene bead layer covered with a thin metal film can be created over a large area by a bottom–up fabrication process. The metal nanodome arrays exhibited unique colorations which can be tuned by the dome diameter ϕ, metal species, and refractive index of the surrounding medium. The measurement of the bulk refractive index sensitivity revealed that the Ag nanodome with ϕ = 500 nm can provide the highest sensitivity of up to 588 nm per refractive index unit. The detection of DNA hybridization was performed by using a bimetallic nanodome consisting of silver and thin gold overlayers and DNA modified gold nanoparticles (AuNPs) for enhancing the sensor signals. Upon the immobilization of AuNPs, the Ag nanodome (ϕ = 200 nm) exhibited a large shift in the resonance wavelength accompanied by a dramatic change in coloration. The analysis of detection sensitivity of DNA hybridization using a model system revealed that colorimetric detection based on hue can be used for the quantitative detection of biomolecules in the same manner as the spectroscopic method with a few pM level of detectable concentration.

Received 21st May 2019
Accepted 3rd August 2019

DOI: 10.1039/c9na00315k

rsc.li/nanoscale-advances

Introduction

In the last three decades, surface plasmon biosensors have become an established analytical tool for biomolecular interactions and sensitive detection of various biomolecules.[1–5] Due to the increasing demands for detection methods of target molecules relating to point of care testing and environmental monitoring, the establishment of portable plasmonic biosensors has emerged as one of the important subjects.[6–11] To miniaturize plasmonic biosensors, implementation of metal nanostructures is a straightforward approach as the resonance conditions of surface plasmons are highly controllable by the geometry of the metal layer. For instance, diffraction gratings coated with a thin metal film have been employed to utilize the nature of propagating surface plasmons called grating coupled surface plasmon resonance (GC-SPR) without using a prism.[10–13] Along with GC-SPR, localized surface plasmon resonance (LSPR) on metal nanostructures has been widely used for biosensor applications.[3,14] Recent progress in plasmonic metamaterials consisting of two or three dimensional metal nanostructure arrays has been providing ways to design high performance plasmonic biosensors.[15,16] Initially, the miniaturization of plasmonic biosensors has been achieved by simplifying the optical setup. Nowadays, the development of smartphone-based plasmonic biosensors is attracting great attention as optical measurements can be performed with the light source and digital cameras integrated in a smartphone by using the appropriate attachment.[7,11,17,18] For example, biomolecular detection was performed by smartphone-based surface plasmon resonance imaging using a sensor chip supporting GC-SPR, and the detection of mouse IgG at the nM level was demonstrated.[18] Similar to conventional plasmonic biosensors, various optical signals can be recorded using a smartphone-based sensing system, such as reflectance and transmittance at a fixed wavelength or spectroscopic readout. Colorimetric detection is one of the attractive methods, which is unique to smartphone-based plasmonic biosensors.[7] In a colorimetric plasmonic biosensor, the immobilization of target molecules onto the sensor surface can be detected as a change in coloration of the sensing spot, quantified by the measurement of changes in RGB values or shift in hue angles in a color space

Department of Applied Chemistry for Environment, School of Science and Technology, Kwansei Gakuin University, Sanda, Japan 669-1337

† Electronic supplementary information (ESI) available: The schematic of the surface modification process of the sensor surface; UV-vis absorption spectra of DNA modified AuNPs; schematic of the optical setup; photographs of Ag nanodome arrays (ϕ = 350 nm) created with various Ag thicknesses; transmission spectra of Ag nanodome arrays recorded at various incident angles; a video of the reversible change in the coloration of Ag nanodome arrays. See DOI: 10.1039/c9na00315k

‡ Present address: Department of Electrical and Electronic Engineering, School of Engineering, Tokyo Institute of Technology, Yokohama, Japan 226-5919, E-mail: toma.m.aa@m.titech.ac.jp

obtained from photographs. Therefore, the camera function of smartphones can be used as it is without using the additional attachments for spectroscopic measurement. Though the idea of colorimetric detection has been adopted in plasmonic biosensors utilizing aggregation of metal nanoparticles in aqueous solution,[19,20] spectroscopic measurement and visual examination are commonly combined for biosensing. On this point, plasmonic coloration from metal nanostructure arrays created on a solid substrate may hold potential for quantitative analysis by RGB values or color space coordinates, as well as the ease of implementation into a lab-on-a-chip device. The color generation of metal nanostructure arrays has been widely studied for plasmonic color printing technology,[21–24] and up to now, several research groups have reported the possibility of plasmonic coloration of metal nanostructure arrays for colorimetric biosensor applications.[7,25–27] Shinohara *et al.* had reported the dramatic change in the coloration of silver nanoparticle sheets due to the immobilization of gold nanoparticles *via* biotin–avidin interactions.[25] Recently, the detection of streptavidin at the sub nM level had been reported by using gold-silver alloy nanodisk arrays.[27] Nevertheless, the reports on colorimetric plasmonic biosensors based on metal nanostructure arrays mainly demonstrated bulk refractive index measurements or the detection of biomolecules in a high concentration range. Furthermore, most colorimetric detection schemes reported the changes of colors in photographs and actual quantitative analysis was performed by spectroscopic methods.

Herein, we report a colorimetric plasmonic biosensor scheme which can be used to perform the quantitative analysis of biomolecules by measuring the hue angle in the HSV (hue, saturation and value) color space obtained from the RGB value of photographs. To create plasmonic coloration, we utilized metal nanodome array structure consisting of a metal coated polystyrene (PS) bead layer which is also referred to as metal semi-shell or metal half shell structures.[28–30] The metal nanodome arrays are considered to be an attractive plasmonic metamaterial, as the structures can be created over a large area (centimeter scale) by a simple and scalable bottom–up nanofabrication process, and their optical properties are controllable by the size of PS beads and components of the metal layer. In this study, we created the metal nanodome arrays by using PS beads with diameters ϕ of 200, 350 and 500 nm and thin metal films, namely those of silver and gold. The fundamental optical properties and sensing performance of the metal nanodome array were investigated by the spectroscopic method and colorimetric method based on the image analysis of the photograph. Specifically, the optical properties of the metal nanodome arrays were investigated by reflectivity measurements, and their plasmonic colorations were evaluated by using hue, saturation and value (HSV) coordinates in a color space. Then, bulk refractive index measurement was carried out by spectroscopic measurement to investigate the fundamental sensing properties of the metal nanodome arrays. For biosensor application, the detection of DNA hybridization was performed by using a bimetallic layer structure by coating the surface of the Ag nanodome with a thin Au overlayer (*ca.* 6 nm thick) to prevent the oxidization of the Ag layer. In addition, DNA modified gold nanoparticles (AuNPs) were used to enhance the sensor signals. The sensor signals induced by the immobilization of DNA-AuNPs *via* DNA hybridization were compared among the Ag nanodome arrays with different dome sizes and Au nanodome arrays (ϕ = 200 nm). The detailed characterization of sensing performance was carried out by using Ag nanodome arrays (ϕ = 200 nm) which exhibited the largest shift in resonance wavelength upon the binding of DNA-AuNPs, accompanied by dramatic changes in the coloration of the sensing spot. Furthermore, quantitative measurement of sensor signals defined by the shift in resonance wavelength as well as hue angles was demonstrated to evaluate the performance characteristics of the colorimetric plasmonic biosensor utilizing Ag nanodome array structures including detection sensitivity.

Experimental

Materials

Carboxylate-coated polystyrene (PS) bead solutions (2.6% w/v, 200, 350 and 500 nm in diameter ϕ) were obtained from Polysciences. Dopamine hydrochloride, ethylene glycol, gold(III) chloride hydrate, Triton X and phosphate buffered saline tablets were purchased from Sigma. Trisodium citrate was obtained from Wako Pure Chemical Co. Three single-stranded DNA (ssDNA) sequences were purchased from Integrated DNA Technologies. The sequences are denoted as Rc30, R30, and T30: Rc30 = 5′-$NH_2(CH_2)_{12}$CGAAATCCAGACACATAAGCACGAACCGAA-3′, R30 = 5′-SH-$(CH_2)_6$-TTCGGTTCGTGCTTATGTGTCTGGATTTCG-3′, and T30 = 5′-NH_2-$(CH_2)_{12}$-(T)30-3′. All the chemicals were used as received.

Fabrication of metal nanodome arrays

Metal nanodome array structures were fabricated by a simple and scalable process as shown in Fig. 1a. First, the PS bead solution was spin coated onto a cleaned glass substrate as described

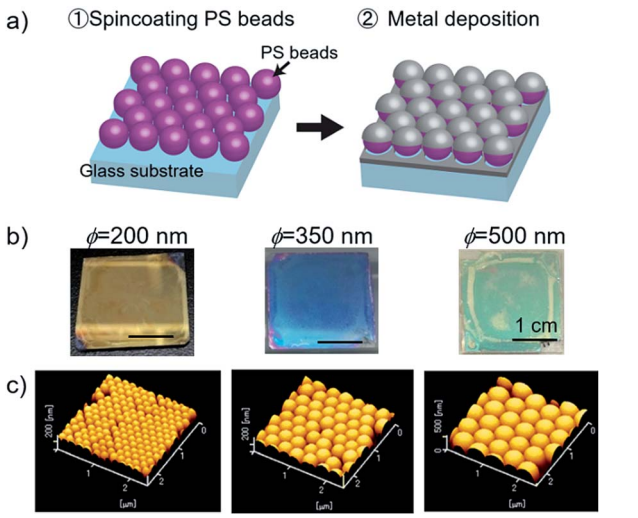

Fig. 1 (a) Schematic of the fabrication process, (b) representative photographs and (c) AFM images of Ag nanodome arrays (left: ϕ = 200 nm, middle: ϕ = 350 nm, right: ϕ = 500 nm).

elsewhere.[31,32] The solvent of the PS bead solution was replaced with a mixed solvent of water and ethanol with a mixing volume ratio of 1 : 3. In an ethanol solution, a spike of Triton X was added as 0.2 v% as a surfactant. The concentration of the PS bead solution was adjusted roughly from 1 w% to 2.5 w% for 200 to 500 nm PS beads, respectively. For the spin coating process, a typical set of conditions (1000 rpm for 6 s) was used. The substrate was placed in a plastic Petri-dish in order to let the solvent dry slowly and PS beads form closely packed layers by a self-assembly process. Ag or Au thin films were deposited by Rf sputtering. A thin Ti layer was used as an adhesion layer of the Ag thin film. The Ag thickness was varied from 30 to 130 nm, but the typical Ag thickness was 53 ± 1 nm. Before conducting experiments, the substrates were annealed at 100 °C on a hotplate for a couple of minutes to improve the adhesion of PS beads onto the glass substrate. For biosensor application, patterned sensing spots were created by using a stencil mask made from a Kapton tape. The diameter of each sensing spot is about 2 mm and seven spots were created on one sensor chip.

Sensor surface functionalization

The sensor surface was modified with single stranded DNA for the detection of DNA hybridization. The surface modification process is described in Fig. S1 in the ESI.† For biosensor application, an additional Au layer (thickness: 6 ± 1 nm) was sputtered on top of the Ag nanodome arrays to prevent the oxidation of the Ag layer in an aqueous environment. Polydopamine chemistry was employed to anchor the amino-terminated single stranded DNA as described elsewhere.[33] After annealing the substrate, a solution of dopamine hydrochloride adjusted to 2 mg mL^{-1} in Tris buffer (10 mM, pH 8.5) was dropped on the sensor surface. After 10 min of incubation, the sensor surface was rinsed with MilliQ water, and dried under a N_2 stream. An amino-terminated ssDNA solution adjusted to 250 μM in PBS was applied onto the sensor spot and then incubated overnight. The sensor surface was rinsed with PBS buffer before measurement.

Synthesis of gold nanoparticles

AuNPs with a diameter of around 15 nm were synthesized by citrate reduction. Briefly, $HAuCl_4$ was dissolved in water (0.26 mM, 19 mL), and sodium citrate dihydrate (20 mM, 1 mL) was then injected into the boiling solution. Afterwards, the reaction solution was continued to boil, until the color of the solution turned red. The AuNP solution was purified by centrifuge separation three times and then stored after re-dispersion in MilliQ water. The ligand exchange of the AuNPs is described in a previous paper.[34] The concentration of AuNPs was set to *ca.* 3 nM by UV-vis absorption spectra using a molar extinction coefficient of 2.7×10^8 M^{-1} cm^{-1}.[33] The UV-vis absorption spectrum is shown in Fig. S2 in the ESI.† As shown in Fig. S2,† the DNA-AuNPs showed the absorption peak induced by LSPR at 525 nm.

Optical setup

A laboratory-built optical setup was used for the reflectivity measurement as shown in Fig. S3 in the ESI.† White light from a tungsten halogen lamp (SLS201/M, Thorlabs) was coupled to an optical fiber (M92L01, 200 μm, 0.22NA, Thorlabs) and collimated by using a collimation mirror (RC08SMA-P01, Thorlabs). A collimated beam was passed through a beam splitter (PDBSH-25.4C1.5, Sigma-Koki) and focused on the sensor surface using a concave lens (SL-SQ-25-150P, Sigma-Koki). The spot size on the sample surface was about 1 mm in diameter. A sensor chip was set to a rotation stage (SGSP-60YAW-0B, Sigma-Koki) to adjust the incident angle to zero degrees. A sensor chip covered with Ag nanodome arrays was fixed to a holder, which was attached to helicoidal post holder and linear stage to adjust the position of the sensing spot. To conduct an experiment in aqueous solution, a flow cell made from a PDMS sheet was placed on the surface of the sensor chip. The sample solution was introduced using an injection syringe, or flowed over the sensor surface using a peristaltic pump. The reflected light was partially reflected by the beam splitter and coupled to an optical fiber by using a condenser lens (F810SMA-635, Thorlabs) connected to a spectrometer (Maya2000, Ocean Optics). Spectrometer control, data acquisition and data analysis were performed using LabVIEW software. An Al mirror (TFA-20C03-10, Sigma-Koki) was used to obtain a reference spectrum. The reflectivity spectra were fitted with a quadratic equation by using the threshold value to determine the reflectivity minimum.

Hue angle measurement

The photograph of the Ag nanodome array was taken using a smartphone camera (Nexus, LG) under the illumination of a fluorescent lamp. The automatic function was selected to adjust the white balance and brightness. The RGB value of the sensor spot was obtained from the photograph by using ImageJ (US National Institutes of Health, http://imagej.nih.gov/ij/) and a function called color histogram. Then, the hue (H), saturation (S) and value (V) were calculated from the RGB values using an algorithm described in the literature.[35]

Results and discussion

Characterization of metal nanodome arrays

When the PS bead layers were coated with the Ag thin film, the Ag nanodome surface exhibited unique coloration depending on the size of the PS beads ϕ. Fig. 1b shows the typical photographs of Ag nanodome arrays created with a 50 nm thick Ag layer. The Ag nanodome array structures were created over the area of a glass slide cut into 2.5 × 2.5 cm^2 indicated as the generation of plasmonic coloration. Ag nanodome arrays exhibited gold (ϕ = 200 nm) and blue (ϕ = 350 nm) colors. As the size of the nanodome enlarged (ϕ = 500 nm), it showed coloration that changes with the viewing angles, indicating the nature of iridescence due to diffraction. When the thickness of the Ag layer was varied, the appearance of Ag nanodome arrays dramatically changed. The photographs of Ag nanodome arrays (ϕ = 350 nm) with various Ag thicknesses are shown in Fig. S4 in the ESI.† As shown in the photographs, the thinner Ag layer with a thickness of 30 nm resulted in the increase of transparency. On the other hand, the coloration faded upon increasing the

thickness of the Ag layer to more than 100 nm. From these observations, we consider that the optimum thickness of the Ag layer to generate vivid coloration is in the range from 40 to 60 nm. Atomic force microscope (AFM) observation was performed to characterize the structure of Ag nanodome arrays. Fig. 1c shows the representative AFM images of the Ag nanodome arrays created with different sizes of PS beads ($\phi = 200$, 350 and 500 nm). From these AFM images, the formation of the closely packed PS bead layer was confirmed. The fundamental optical properties of the Ag nanodome arrays were investigated by reflectivity measurements at vertical incidence. Fig. 2a–d show the reflectivity spectra and photograph of Ag and Au nanodome arrays in contact with air and water. The reflectivity spectra of each metal nanodome array exhibited reflectivity drops associated with resonant excitation of surface plasmons, which vary with the size of the nanodome. The red shift of the resonance wavelength λ_m of the main dip occurred as the size of the Ag nanodome increased, which is in good agreement with the literature.[29,36] The resonance curves of the Ag nanodome array ($\phi = 350$ and 500 nm) exhibited two dips, indicating that these metal nanodome array structures have multiple optical modes. The appearance of additional features in the shorter wavelength region was likely due to the far field diffraction and photonic mode of PS beads.[36] The Au nanodome arrays ($\phi = 200$ nm) exhibited resonance at a longer wavelength with respect to the Ag nanodome arrays with the same dome diameter, and exhibited red color in air. When a water droplet was applied on top of the metal nanodome array surface, deformation of reflectivity spectra occurred accompanied by a dramatic color change. The deformation of the reflectivity spectra was dominantly due to the red shift of the resonance wavelength λ_m caused by the increase of the refractive index of the surrounding medium from air to water. The resonance wavelength λ_m of the main dip and hue, saturation and value (HSV) coordinates in a color space are summarized in Table 1. The saturation and value are defined in the range from 0 to 1. Note that the chroma and brightness are correlated to saturation and value, respectively.

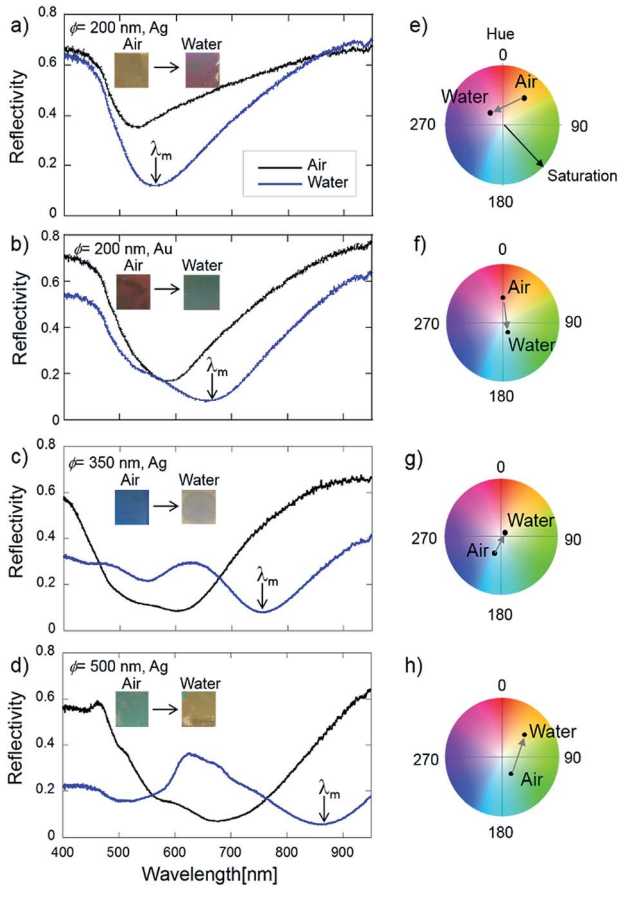

Fig. 2 Reflectivity spectra and photograph of Ag and Au nanodome arrays taken in air and water (left column), and the coloration scale (right column). Metal species and the size of PS beads are (a and e) Ag ($\phi = 200$ nm), (b and f) Au ($\phi = 200$ nm), (c and g) Ag ($\phi = 350$ nm), and (d and h) Ag ($\phi = 500$ nm).

The Ag nanodome array ($\phi = 200$ nm) exhibited the smallest shift in resonance wavelength λ_m of *ca.* 30 nm from air to water in the reflectivity measurement. On the other hand, the coloration dramatically changed from yellow to red along with the shift of hue angles in the counterclockwise direction from 40 to 314 degrees (Δhue = 86 degrees). In the case of the Au nanodome array ($\phi = 200$ nm), the shift in the resonance wavelength was 64 nm, and the shift in hue reached about 150 degrees. The shift of the resonance wavelength λ_m increased to 168 nm for the Ag nanodome array ($\phi = 350$ nm). However, the bluish color in air faded upon applying a water drop, indicated by the decrease of saturation from 0.3 to 0.1 as well. We consider that this is the result of the shift of the resonance wavelength to the near infrared wavelength region which led to flattening of the reflectivity spectra in the visible wavelength region. The largest Ag nanodome array ($\phi = 500$ nm) exhibited a shift in the resonance wavelength as high as 173 nm, the color turned from light green to yellow with a shift in the hue angle of 105 degrees. Nevertheless, the coloration changes with the viewing angle. The angle dependent optical properties of Ag nanodome arrays were observed by the transmission spectra recorded at various incident angles. As shown in Fig. S5 in the ESI,† the peak wavelength shifted as the incident angle increased for the large Ag nanodome arrays ($\phi = 500$ nm). As the size of the nanodome decreased, the peak shift was not significant. Based on the spectroscopic measurements, the larger Ag nanodome arrays exhibited higher responses with shifts in the resonance wavelength. On the other hand, Ag and Au nanodome arrays ($\phi = 200$ nm) exhibited vivid coloration both in air and an aqueous

Table 1 Summary of resonance wavelengths and HSV coordinates in the color space of the metal nanodome array

		λ_m [nm]		HSV coordinate	
ϕ [nm]	Metal	In air	In water	In air	In water
200	Ag	532	560	(40, 0.56, 0.79)	(314, 0.28, 0.59)
200	Au	586	650	(2, 0.43, 0.69)	(150, 0.21, 0.44)
350	Ag	617	785	(201, 0.30, 0.55)	(43, 0.10, 0.63)
500	Ag	677	850	(147, 0.31, 0.55)	(42, 0.57, 0.50)

environment, indicating their potential for colorimetric detection.

The change in coloration of metal nanodome arrays caused by the increase of the refractive index of the surrounding medium quickly occurred and was reversible. A video in the ESI† shows that the coloration of the Ag nanodome arrays (ϕ = 200 nm) immediately changed from yellow to purple when water was applied to the surface. Fig. 3 shows the sketch of the sensor chip and the sequential photographs. From the photographs, it can be seen that the coloration of Ag nanodome arrays returned to the original color soon after the water was removed.

Bulk refractive index sensitivity

As the fundamental characteristics of Ag and Au nanodome arrays, bulk refractive index sensitivity was investigated. In this experiment, we evaluate the bulk refractive index sensitivity by spectroscopic measurements, namely reflectivity spectra. Shifts in resonance wavelength λ_m were recorded as sensor signals upon the injection of aqueous solution containing ethylene glycol with different mixing ratios (0, 5, 10, 20 and 30 v%). The resonance wavelength was defined by fitting the reflectivity spectra in Fig. 2 with a quadratic function with a threshold value. A typical sensor response taken with the Ag nanodome array (ϕ = 200 nm) against the injection of the sample solution is shown in Fig. 4a. As shown in Fig. 4a, the resonance wavelength immediately shifted and reached a plateau when the sample solution was injected. The same experiments were performed for other Ag nanodome arrays (ϕ = 350 and 500 nm) and Au nanodome arrays (ϕ = 200 nm), and the shifts in the resonance wavelength $\Delta\lambda_m$ against the increase of the bulk refractive index ΔRI are plotted in Fig. 4b. The measurement was performed more than three times by changing the measurement spots to obtain the standard deviation denoted as error bars. The wavelength dependent refractive indices of water and ethylene glycol were obtained from ref. 37. As shown in Fig. 4b, the linear relationships between the shift in the resonance wavelength and the bulk refractive index changes were observed for the all of Ag nanodome arrays. The bulk refractive index sensitivities were obtained as slopes of the linear fit, and were 162, 497 and 588 nm per refractive index unit (nm per RIU) for the Ag nanodome with ϕ = 200, 350 and 500 nm, respectively. The Au nanodome arrays (ϕ = 200 nm) resulted in a better bulk RI sensitivity (264 nm per RIU) than that of Ag nanodome arrays (ϕ = 200 nm). As discussed in the previous section, the bulk refractive index sensitivity improved as the dome diameter increased. Considering that the typical bulk RI sensitivities of localized surface plasmon sensors are in the range of 100 to 1000 nm per RIU,[34,38,39] the as-fabricated Ag nanodome arrays provide a reasonable bulk RI sensitivity. Regarding the metal nanostructures similar to the Ag nanodome arrays, a lower bulk RI sensitivity of around 60 to 70 nm per RIU was reported.[40,41] These reported studies were performed using a metal nanostructure created with the smaller dielectric nanospheres (ϕ 100

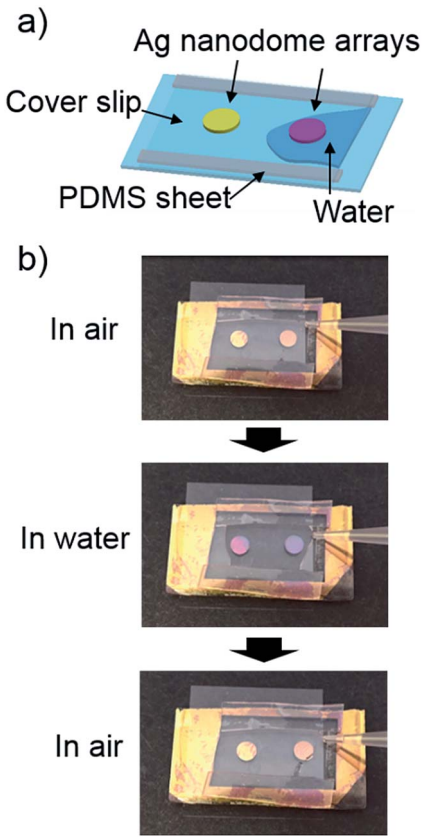

Fig. 3 (a) A sketch of the sensor chip consisting of two sensing spots with Ag nanodome arrays (ϕ = 200 nm) and a chamber to apply water. (b) Sequential photographs of the sensor chip upon water application and removal.

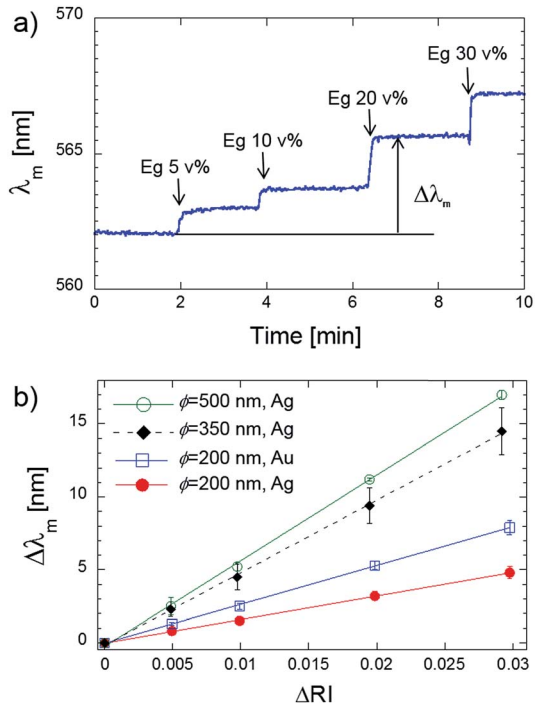

Fig. 4 (a) Real time measurement of sensor responses against the injection of an ethylene glycol solution with different concentrations. (b) Quantitative plot of $\Delta\lambda_m$ against ΔRI.

nm). This effect of the size of Ag nanodome arrays on the refractive index sensitivity is in agreement with other studies performed with Au nanorings and Au nanodiscs.[38,42]

A biosensor for the detection of DNA hybridization

To characterize the performance of the biosensor using metal nanodome arrays, the detection of DNA hybridization was performed. As described in the Experimental section, the surface of Ag nanodome arrays was coated with a thin Au layer to protect them from oxidation. It is noteworthy that the optical properties of Ag nanodome arrays were almost retained upon the deposition of the Au layer with a thickness of around 6 nm. After immobilization of 30-mer single stranded DNA (Rc30) onto the sensor surface, a flow cell made with a PDMS sheet was attached to the sensor surface. The solution containing AuNPs modified with complementary DNA to Rc30 (R30) was flowed over the sensor surface for 40 min by using a peristaltic pump and then rinsed with PBS. The reflectivity spectra and photographs of Ag nanodome arrays (ϕ = 200 nm) taken before and after the immobilization of DNA-AuNPs through DNA hybridization are shown in Fig. 5a. The immobilization of DNA-AuNPs onto the Ag nanodome array surface induced a large shift in the resonance wavelength of 49 nm accompanied by a dramatic change in coloration from purplish-red to greenish-blue. The initial hue of the sensing spot was 325 degrees. The hue angles shifted to the counter clockwise direction in the same manner as the bulk refractive index changes, and the shift amount reached as high as 130 degrees. In the case of the Au nanodome array (ϕ = 200 nm), the shift in the resonance wavelength was suppressed to 35 nm, and the change in coloration was not significant with respect to the Ag nanodome array structure. The optical properties of Ag nanodome arrays were mostly retained upon depositing the thin Au overlayer. The same experiments were carried out for the other Ag nanodome arrays (ϕ = 350 and 500 nm), and the reflectivity spectra are shown in Fig. 4c–d. The shift amount of the resonance wavelength upon immobilization of DNA-AuNPs is summarized in Table 2 with the results of the bulk RI sensitivity. The shift of the resonance wavelength was averaged over at least three different sensor chips to estimate the standard deviation. Interestingly, the sensor response against the binding of DNA-AuNPs exhibited a contradictory trend to the bulk RI sensitivity. For instance, the maximum shift in the resonance wavelength was obtained with the Ag nanodome array with ϕ = 200 nm, which resulted in the lowest bulk RI sensitivity. Furthermore, only this Ag nanodome array exhibited color changes due to the immobilization of DNA-AuNPs, and even the deformation of the reflectivity spectra of Ag nanodome arrays (ϕ = 350 and 500 nm) was also observed in the visible wavelength region. Though the local refractive index sensitivity is not always proportional to the bulk refractive index sensitivity,[43] we consider that the plasmonic coupling between the Ag nanodome array (ϕ = 200 nm) and AuNPs induced the higher optical responses. As shown in the reflectivity spectra in Fig. 5a, the resonance band of Ag nanodome arrays (ϕ = 200 nm) overlaps with that of the LSPR of DNA-AuNPs having an absorption peak at 525 nm. The plasmonic fields may interact in the same manner as a dimer of metal nanoparticles

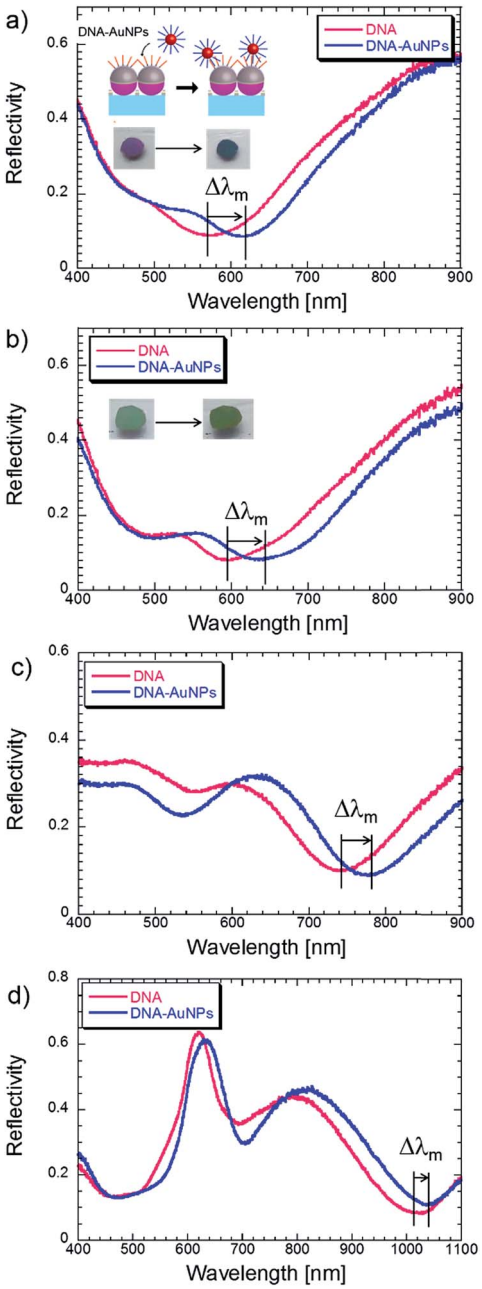

Fig. 5 Reflectivity spectra recorded before and after the immobilization of DNA-AuNPs. (a) Ag nanodome (ϕ = 200 nm), (b) Au nanodome (ϕ = 200 nm), (c) Ag nanodome (ϕ = 350 nm), and (d) Ag nanodome (ϕ = 500 nm).The photographs of sensor spots are inserted in the plot of Ag and Au nanodomes (ϕ = 200 nm).

which induces the large shift in the resonance wavelength.[44] The distance between the surface of the Ag nanodome and AuNPs was estimated to be 14 nm. As the plasmonic field of metal nanospheres is proportional to their diameter (about 15 nm), we consider that plasmonic coupling can occur in the experimental systems used in this study.

For further experiments, we focus on the Ag nanodome arrays with ϕ = 200 nm. In the next experiments, the detection sensitivity of DNA-hybridization using a combination of Ag

Table 2 Comparison of bulk refractive index sensitivities, and the sensor responses against the binding of DNA-AuNPs of metal nanodome arrays

ϕ [nm]	Metal	Bulk RI sensitivity [nm per RIU]	$\Delta\lambda_m$ [nm]
200	Ag	162	49 ± 9
200	Au	264	35 ± 5
350	Ag	497	35 ± 3
500	Ag	588	21 ± 3

nanodome arrays ($\phi = 200$ nm) and DNA-AuNPs was evaluated. Here, we used the patterned sensor chips and a model system to perform multiple measurements at the same time. In particular, the surface coverage of a model target ssDNA was controlled by creating mixed ssDNA monolayers containing Rc30 and T30 on the Ag nanodome array surface instead of varying the concentration of the target ssDNA.[33,34,45,46] Rc30 has a complementary sequence to the ssDNA (R30) anchored to AuNPs, and acts as a model of the target DNA. T30 has a non-complementary sequence to both Rc30 and R30, and therefore the immobilization of DNA-AuNPs does not occur. Here, we assume that the probability of immobilization of Rc30 and T30 onto the PDA surface *via* amino-groups is equal,[45] and the surface coverage of Rc30 (%Rc30) can be controlled by the mixing ratio of Rc30 and T30 in the solution applied to the sensor surface. As shown in Fig. 6a, individual sensing spots were modified with Rc30 and T30 with different mixture ratios. In this case, the mixture ratio of Rc30 and T30 was varied as 0 : 100, 0.1 : 99.9, 0.2 : 99.8, 1 : 99, 10 : 90, and 100 : 0%, indicated by the numbers in the sensing spots in the diagram. To simplify the expression, we described the mixture ratio of Rc30 as its relative surface coverage. The photographs were taken before and after the immobilization of DNA-AuNPs. From the photographs, the visible color changes of the sensing spots were observed depending on the surface coverage of Rc30. Though the color change was not distinguishable for the control spot fully covered with T30, it could be observed for the sensor spot containing Rc30 with the surface coverage down to 0.1%. As it can be seen in the photograph in Fig. 6a, the coloration of the Ag nanodome arrays was not perfectly homogeneous. It was caused by the inhomogeneity of the arrangement of Ag nanodome arrays, such as the formation of multilayers and disordered structures. Therefore, we reduced the spot size of incident light to about 1 mm in diameter to suppress the broadening of the reflectivity spectra and to select the sensing areas exhibiting comparable optical properties. In this experiment, the typical resonance wavelength λ_m and hue angle of the Ag nanodome arrays were 563 ± 14 nm and 324 ± 22 degrees, respectively. To obtain the quantitative plot, the surface coverage of Rc30 was varied as 0, 0.0025, 0.01, 0.05, 0.1, 1, 10, and 100%. The experiments were repeated more than four times ($n \geq 4$) by using different sensor chips in order to determine the standard deviation of the sensor signals. For spectroscopic measurements, the reflectivity spectra were sequentially recorded from each sensing spot by moving a sensor chip using a liner stage.

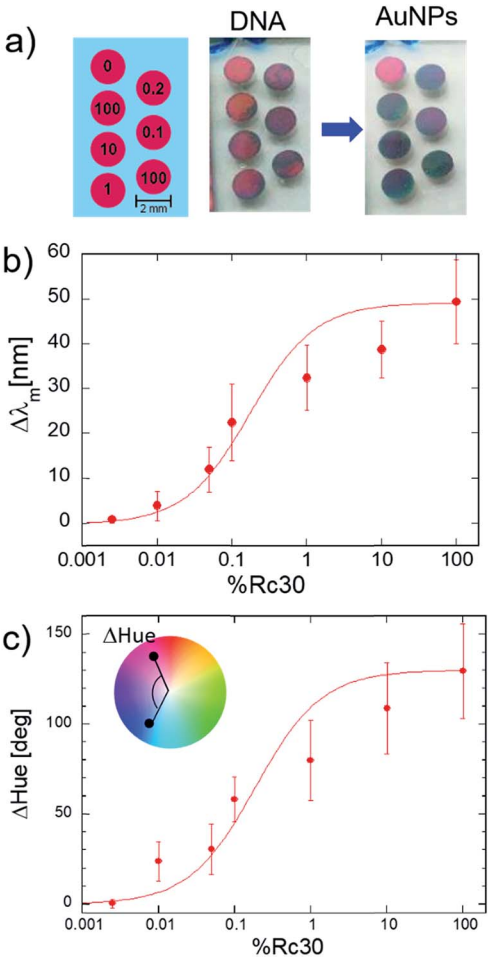

Fig. 6 (a) (Left) Sketch of the sensing spots and photographs of the sensing spots taken before (middle) and after immobilization of DNA-AuNPs (right). The quantitative plot of (b) shift amount of the resonance wavelength $\Delta\lambda_m$ and (c) shift in the hue angle Δhue against the relative surface coverage of Rc30, %Rc30.

The standard deviation σ of the resonance wavelength and the hue angle from the same sensing spot were determined to be 0.7 nm and 4.7 degrees. After flowing a solution containing DNA-AuNPs and rinsing with PBS, reflectivity spectra were recorded again from each sensing spot, and then the shifts in the resonance wavelength were obtained. The quantitative plot obtained by spectroscopic measurement is shown in Fig. 6b. When the sensor surface is covered with control DNA (T30), the $\Delta\lambda_m$ became negligible ($\Delta\lambda_m = -0.3$ nm) which is below the standard deviation σ of the measurement ($\sigma = 0.7$ nm). A clear shift of the resonance wavelength ($\Delta\lambda_m = 3.9$ nm) was observed when the surface coverage of Rc30 reached 0.01%. A dramatic change in the $\Delta\lambda_m$ occurred up to 1%, and then the change of $\Delta\lambda_m$ became moderate. For colorimetric detection, we focused on the shift in hue angles of each sensing spot. The absolute values of shift in the hue angle are summarized in Fig. 6c. As shown in Fig. 6c, the quantitative plot obtained by the colorimetric method resulted in a good agreement with that taken by the spectroscopic method. The change in hue angles can be

observed for a surface coverage down to 0.01%, and a dramatic shift in the hue angle occurs in the range of 0.01 to 1%. We consider that the quantitative analysis of biomolecules is possible based on colorimetric detection by using the combination of Ag nanodome arrays and AuNPs. The detectable surface coverage of Rc30 was estimated as the intersection of the fitting curve and three times the standard deviation described as 3σ. The determined LOD was 0.03% of the surface coverage of Rc30. Here, the obtained data may contain a relatively large error bar as this experiment was performed under a fluorescent lamp using a smartphone camera without specialized housing. Therefore, we expect that the detection sensitivity can be improved by optimizing the setup for colorimetric detection. After performing the end-point measurement to compare spectroscopic and colorimetric detection, we characterized the detailed sensor responses for the low surface coverage of Rc30 by real time *in situ* measurement of the resonance wavelength λ_m. In this experiment, the surface coverage of Rc30 was varied as 0, 0.0025, 0.01, 0.05 and 0.1%, and the shift in the resonance wavelength $\Delta\lambda$ was recorded as a function of time as shown in Fig. 7a. The $\Delta\lambda$ increased after the injection of DNA-AuNPs for the sensor surface containing DNA-Rc30 (% Rc30 $\geq$ 0.0025), where no detectable wavelength shift was observed for the control. After 40 min from the introduction of the AuNP solution, the sensor surface was rinsed with PBS and the shift of the resonance wavelength $\Delta\lambda_k$ was recorded. The quantitative plot of the $\Delta\lambda_k$ as a function of surface coverage of Rc30 (%Rc30) is shown in Fig. 7b. In this range of surface coverage, the sensor response follows a liner relationship. From the standard deviation of the sensor diagram ($\sigma_k = 0.04$ nm), it is reasonable to consider that the 0.0025% of %Rc30 resulting in a $\Delta\lambda_k$ of 0.58 nm is detectable surface coverage.

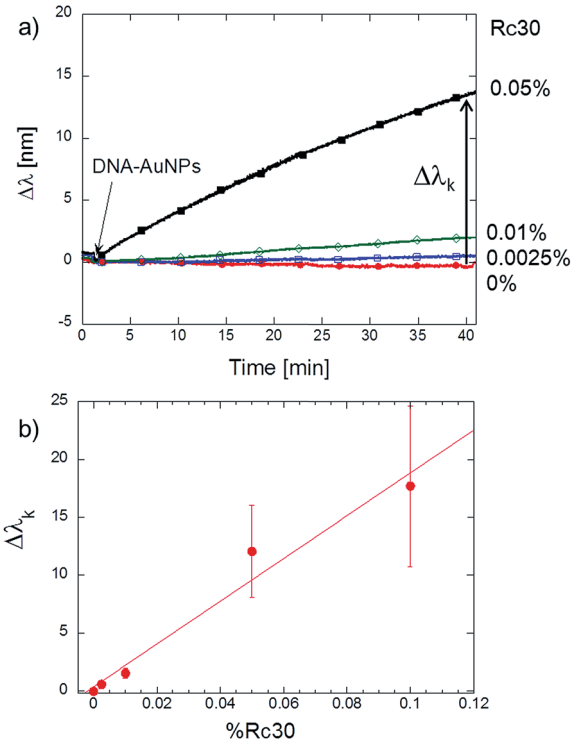

Fig. 7 (a) Real time measurement of the shift in the resonance wavelength $\Delta\lambda$ against the injection of the DNA-AuNPs. (b) Quantitative plot of $\Delta\lambda_k$ against %Rc30.

Here, we introduce a simple assumption to estimate the detectable concentration of Rc30 from its surface coverage.[33,34,45] The surface coverage θ of ssDNA immobilized on the sensor surface *via* DNA hybridization can be described using the Langmuir isotherm equation, using the concentration of target DNA C and the affinity constant of DNA hybridization K_{ads}. When the concentration of DNA C is low enough and the relation $K_{ads} \cdot C \ll 1$, the equation can be described as $\theta = K_{ads} \cdot C$. In our experiment, we assume that the surface coverage of Rc30 is nearly equal to the mixing ratio of Rc30 according to the literature.[45] By using the Langmuir adsorption constant K_{ads} of 10^8 M^{-1},[33] the concentration of ssDNA is estimated to be about 250 fM from the surface coverage θ of Rc30 (0.0025%). Therefore, we consider that the detection of target DNA at the sub pM level is possible by spectroscopic measurement. In the case of colorimetric measurement, the detectable minimum surface coverage of Rc30 was 0.03%. The detectable concentration of DNA is estimated to be about 3 pM.

Up to here, we have shown that the presented biosensor scheme based on a combination of Ag nanodome arrays (ϕ = 200 nm) and DNA-AuNPs can detect DNA hybridization for a relative surface coverage as low as 0.0025 and 0.03% by the spectroscopic method and colorimetric method, respectively. There are several studies reporting the detection sensitivity of DNA hybridization by using similar samples performed using different optical systems. For instance, the conventional SPR measurement based on propagating surface plasmons could provide a detectable surface coverage as low as 0.1%.[33] By using a localized surface plasmon biosensor on gold nanoring arrays, the minimum detectable surface coverage was 0.5%.[34] With respect to these plasmonic biosensors, the Ag nanodome arrays may provide advanced detection sensitivity through a much simpler detection scheme. The detection sensitivity of the presented plasmonic biosensor may not reach that of surface plasmon-enhanced fluorescence (SPF) biosensors or other ultrasensitive plasmonic biosensor schemes in which much complicated metal nanostructures or optical setups are required.[12,47,48] The presented biosensor scheme holds potential for the rapid and sensitive detection of biomolecules without using specialized equipment.

Conclusions

In this study, we have proposed a sensitive plasmonic biosensor scheme based on colorimetric detection which can perform quantitative detection of biomolecules expressed by hue angles. As the origin of plasmonic coloration, silver and gold nanodome arrays consisting of a polystyrene bead layer coated with thin metal films were created over a large area based on a bottom–up nanofabrication technique. The Ag nanodome arrays exhibited unique coloration varying with the dome size defined by the PS bead diameter. To evaluate the optical properties and sensing performance of the Ag and Au nanodome

array, both spectroscopic measurements based on reflectivity spectra and colorimetric detection by image analysis of the photograph taken using a smartphone camera were carried out. The characterization of the bulk refractive index sensitivity revealed that the bulk RI sensitivity improved as the size of the nanodome enlarged, and reached 588 nm per RIU for the Ag nanodome with $\phi = 500$ nm. In contrast, the smallest Ag nanodome arrays ($\phi = 200$ nm) could provide the highest sensor signals for detection of DNA-hybridization by using DNA modified AuNPs by both spectroscopic and colorimetric measurements. The experimental results implied that the plasmonic coupling between Ag nanodome arrays and DNA-AuNPs plays an important role in generating a large shift in the resonance wavelength accompanied by changes in coloration of the Ag nanodome arrays. The detection sensitivity for DNA hybridization was evaluated with a model system by controlling the relative surface coverage of the target DNA on the sensor surface. From the plot of sensor signals against the surface coverage of target DNA, it was revealed that a reasonable quantitative measurement can be performed based on colorimetric detection by using a smartphone camera. The detectable surface coverage of target DNA was 0.0025 and 0.03% by the spectroscopic and colorimetric method, respectively, which correspond to a concentration in the sub to few pM level. To the best of our knowledge, this is the first demonstration of a colorimetric plasmonic biosensor utilizing metal nanostructure arrays, enabling sensitive and quantitative detection of biomolecules by hue angle measurement. As the presented biosensor scheme can be versatile for the detection of various biomolecules by modifying the sensor surfaces with other biorecognition elements, our future work will include the demonstration of immunoassays for the detection of disease related biomolecules such as biomarkers and pathogens.

Conflicts of interest

There are no conflicts to declare.

Acknowledgements

This work was supported by JSPS KAKENHI Grant Numbers, JP15H06766 in Research Activity Start-up, JP16H02092 in Scientific Research (A) and MEXT KAKENHI Grant Number JP17H05273 in Scientific Research on Innovative Areas "Photosynergetics".

Notes and references

1 J. Homola, *Chem. Rev.*, 2008, **108**, 462.
2 M. Bauch, K. Toma, M. Toma, Q. Zhang and J. Dostalek, *Plasmonics*, 2014, **9**, 781.
3 M. E. Stewart, C. R. Anderton, L. B. Thompson, J. Maria, S. K. Gray, J. A. Rogers and R. G. Nuzzo, *Chem. Rev.*, 2008, **108**, 494.
4 B. Liedberg, C. Nylander and I. Lundstrom, *Biosens. Bioelectron.*, 1995, **10**, R1.
5 O. Tokel, F. Inci and U. Demirci, *Chem. Rev.*, 2014, **114**, 5728.
6 A. G. Brolo, *Nat. Photonics*, 2012, **6**, 709.
7 X. H. Wang, T. W. Chang, G. H. Lin, M. R. Gartia and G. L. Liu, *Anal. Chem.*, 2017, **89**, 611.
8 K. Toma, M. Vala, P. Adam, J. Homola, W. Knoll and J. Dostalek, *Opt. Express*, 2013, **21**, 10121.
9 A. Prasad, J. Choi, Z. Jia, S. Park and M. R. Gartia, *Biosens. Bioelectron.*, 2019, **130**, 185.
10 J. L. Zhang, I. Khan, Q. W. Zhang, X. H. Liu, J. Dostalek, B. Liedberg and Y. Wang, *Biosens. Bioelectron.*, 2018, **99**, 312.
11 C. Lertvachirapaiboon, A. Baba, K. Shinbo and K. Kato, *Anal. Methods*, 2018, **10**, 4732.
12 M. Toma, S. Izumi and K. Tawa, *Analyst*, 2018, **143**, 858.
13 K. Tawa, M. Umetsu, T. Hattori and I. Kumagai, *Anal. Chem.*, 2011, **83**, 5944.
14 A. Ricciardi, A. Crescitelli, P. Vaiano, G. Quero, M. Consales, M. Pisco, E. Esposito and A. Cusano, *Analyst*, 2015, **140**, 8068.
15 A. E. Cetin, A. F. Coskun, B. C. Galarreta, M. Huang, D. Herman, A. Ozcan and H. Altug, *Light: Sci. Appl.*, 2014, **3**, e122.
16 A. Leitis, A. Tittl, M. Liu, B. H. Lee, M. B. Gu, Y. S. Kivshar and H. Altug, *Sci. Adv.*, 2019, **5**, eaaw2871.
17 Y. Liu, Q. Liu, S. Chen, F. Cheng, H. Wang and W. Peng, *Sci. Rep.*, 2015, **5**, 1.
18 H. Guner, E. Ozgur, G. Kokturk, M. Celik, E. Esen, A. E. Topal, S. Ayas, Y. Uludag, C. Elbuken and A. Dana, *Sens. Actuators, B*, 2017, **239**, 571.
19 L. H. Tang and J. H. Li, *ACS Sens.*, 2017, **2**, 857.
20 P. Chen, X. Liu, G. Goyal, T. Nhung Thi, J. C. S. Ho, Y. Wang, D. Aili and B. Liedberg, *Anal. Chem.*, 2018, **90**, 4916.
21 K. Kumar, H. G. Duan, R. S. Hegde, S. C. W. Koh, J. N. Wei and J. K. W. Yang, *Nat. Nanotechnol.*, 2012, **7**, 557.
22 R. Mudachathi and T. Tanaka, *Sci. Rep.*, 2017, **7**, 1199.
23 X. L. Zhu, C. Vannahme, E. Hojlund-Nielsen, N. A. Mortensen and A. Kristensen, *Nat. Nanotechnol.*, 2016, **11**, 325.
24 L. Wang, R. J. H. Ng, S. Safari Dinachali, M. Jalali, Y. Yu and J. K. W. Yang, *ACS Photonics*, 2016, **3**, 627.
25 S. Shinohara, D. Tanaka, K. Okamoto and K. Tamada, *Phys. Chem. Chem. Phys.*, 2015, **17**, 18606.
26 M. R. Gartia, A. Hsiao, A. Pokhriyal, S. Seo, G. Kulsharova, B. T. Cunningham, T. C. Bond and G. L. Liu, *Adv. Opt. Mater.*, 2013, **1**, 68.
27 I. Misbah, F. S. Zhao and W. C. Shih, *ACS Appl. Mater. Interfaces*, 2019, **11**, 2273.
28 Z. Yi, G. Niu, J. Luo, X. Kang, W. Yao, W. Zhang, Y. Yi, Y. Yi, X. Ye, T. Duan and Y. Tang, *Sci. Rep.*, 2016, **6**, 32314.
29 K. Sugawa, T. Tamura, H. Tahara, D. Yamaguchi, T. Akiyama, J. Otsuki, Y. Kusaka, N. Fukuda and H. Ushijima, *ACS Nano*, 2013, **7**, 9997.
30 T. Endo, K. Kerman, N. Nagatani, H. M. Hiepa, D. K. Kim, Y. Yonezawa, K. Nakano and E. Tamiya, *Anal. Chem.*, 2006, **78**, 6465.
31 M. Toma, G. Loget and R. M. Corn, *ACS Appl. Mater. Interfaces*, 2014, **6**, 11110.
32 A. R. Halpern and R. M. Corn, *ACS Nano*, 2013, **7**, 1755.

33 J. B. Wood, M. W. Szyndler, A. R. Halpern, K. Cho and R. M. Corn, *Langmuir*, 2013, **29**, 10868.
34 M. Toma, K. Cho, J. B. Wood and R. M. Corn, *Plasmonics*, 2014, **9**, 765.
35 A. R. Smith, *ACM SIGGRAPH Computer Graphics*, 1978, **12**, 12.
36 C. Farcau and S. Astilean, *Appl. Phys. Lett.*, 2009, **95**, 193110.
37 H. El-Kashef, *Phys. B*, 2000, **279**, 295.
38 E. M. Larsson, J. Alegret, M. Kall and D. S. Sutherland, *Nano Lett.*, 2007, **7**, 1256.
39 K. M. Mayer and J. H. Hafner, *Chem. Rev.*, 2011, **111**, 3828.
40 M. Himmelhaus and H. Takei, *Sens. Actuators, B*, 2000, **63**, 24.
41 D. K. Kim, S. M. Yoo, T. J. Park, H. Yoshikawa, E. Tamiya, J. Y. Park and S. Y. Lee, *Anal. Chem.*, 2011, **83**, 6215.
42 P. Hanarp, M. Kall and D. S. Sutherland, *J. Phys. Chem. B*, 2003, **107**, 5768.
43 M. Piliarik, H. Sipova, P. Kvasnicka, N. Galler, J. R. Krenn and J. Homola, *Opt. Express*, 2012, **20**, 672.
44 N. J. Halas, S. Lal, W. S. Chang, S. Link and P. Nordlander, *Chem. Rev.*, 2011, **111**, 3913.
45 Y. L. Chen, A. Nguyen, L. F. Niu and R. M. Corn, *Langmuir*, 2009, **25**, 5054.
46 A. R. Halpern, J. B. Wood, Y. Wang and R. M. Corn, *ACS Nano*, 2014, **8**, 1022.
47 J. Dostalek and W. Knoll, *Biointerphases*, 2008, **3**, FD12.
48 K. Tawa, F. Kondo, C. Sasakawa, K. Nagae, Y. Nakamura, A. Nozaki and T. Kaya, *Anal. Chem.*, 2015, **87**, 3871.